Electronic Supplementary Material (ESI) for Journal of Materials Chemistry A.
This journal is © The Royal Society of Chemistry 2022

Electronic Supplementary Information (ESI)

Stable Zr(IV) coordination polymers with electroactive metal-terpyridine units for enhanced electrochemical sensing dopamine

Tingting Yan,‡ Xiao-Yu Zhang,‡ Yue Zhao and Wei-Yin Sun*

Coordination Chemistry Institute, State Key Laboratory of Coordination Chemistry, School of Chemistry and Chemical Engineering, Nanjing National Laboratory of Microstructures, Collaborative Innovation Center of Advanced Microstructures, Nanjing University, Nanjing 210023, China

* Corresponding Author. Email address: sunwy@nju.edu.cn

‡ T. T. Y. and X. Y. Z. contributed equally to this work.

Experimental Section

Materials and reagents. All chemicals were purchased from commercial sources and used without further treatment. Dopamine (DA), uric acid (UA), ascorbic acid (AA), glucose (Glu), L-cysteine (Cys), glutathione (GSH), H_2O_2 (30%), $NaNO_2$, lactic acid, citric acid, sodium bicarbonate, urea, calcium chloride, sodium chloride, magnesium sulfate, sodium sulfate, potassium dihydrogen phosphate, dipotassium hydrogen phosphate and ammonium chloride were purchased from Sinopharm Chemical Reagent Co., Ltd (China). Nafion solution (5 wt%) was obtained from Fortune Energy Technology Co., LTD (Suzhou, China). 0.1 M phosphate buffered saline (PBS) was prepared using $Na_2HPO_4 \cdot 12H_2O$ and KH_2PO_4.

Apparatus. Scanning electron microscope (SEM) images were obtained on a Hitachi S-4800 field emission scanning electron microscope and the surface composition of the sample was examined by energy-dispersive X-ray spectroscopy (EDS) attached to SEM. Powder X-ray

diffraction (PXRD) data were collected on a Bruker D8 Advance X-ray diffractometer with a Cu-Kα (λ = 1.5418 Å) radiation source, in which the X-ray tube was operated at 40 kV and 40 mA. Thermogravimetric analyses (TGA) were performed on a Mettler-Toledo thermal analyzer in a N_2 atmosphere at a heating rate of 10 °C min^{-1}. X-ray photoelectron spectroscopy (XPS) measurements were carried out on an ESCALAB 250XI high-performance electron spectrometer with monochromated Al Kα radiation (*hv* = 1486.7 eV) as the excitation source. Zeta potential measurements were collected using the Malvern Zetasizer Nano. The inductively coupled plasma optical emission spectrometry (ICP-OES) measurements were performed on an Aglient 5110 instrument.

Synthesis of electroactive ligands and their CPs. 4′-(4-Methoxycarbonylphenyl)-2,2′:6′,2″terpyridine (Hcptpy) and $Ni(cptpy)_2$ (**Ni-L**) were synthesized according to the published procedure,[1] and $[Ni_2Zr_2(HCOO)_8(cptpy)_4]_3 \cdot 8DMF \cdot 4.7H_2O$ (**Ni-CP**) was obtained according to our previous work.[2] **Fe-L**[3] and $[FeZr(HCOO)_4(cptpy)_2] \cdot 0.3DMF \cdot 4.4H_2O$ (**Fe-CP**) were synthesized by the same procedure used for the preparation of **Ni-L** and **Ni-CP** except that $Fe(NO_3)_3 \cdot 9H_2O$ was used instead of $Ni(OAc)_2 \cdot 4H_2O$. **Fe-CP**: Anal. Calcd for $C_{48.9}H_{42.9}FeN_{6.3}O_{16.7}Zr$: C, 51.84; H, 3.79; N, 7.78%; Found: C, 51.84; H, 3.63; N, 7.66%.

X-ray crystallography. Single-crystal X-ray diffraction data were collected on a Bruker D8 Venture diffractometer with graphite-monochromated Ga Kα radiation (λ = 1.34139 Å). The integration of diffraction data and intensity corrections for the Lorentz and polarization effects were performed by using the SAINT program.[4] Semi-empirical absorption corrections were applied using the SADABS program.[5] The structures were solved by direct methods with SHELXT-2014, expanded by subsequent Fourier-difference synthesis, and all the non-hydrogen atoms were refined anisotropically on F^2 using the full-matrix least-squares technique using the SHELXL-2018 crystallographic software package.[6] The reported refinements are of the guest-free structures obtained by the SQUEEZE routine, and the results were attached to the CIF files.

The free solvents molecules in the unit cell have been taken into account by the SQUEEZE option of the PLATON program.[7] The final chemical formula of **Fe-CP** was obtained based on volume/count electron analysis and TGA (Fig. S1). The details of crystal parameters, data collection and refinements for **Fe-CP** is listed in Table 1.

Measurements of zeta potential. 100 μL of 1 mg the **Fe-L**, **Ni-L**, **Fe-CP** or **Ni-CP** in 1 mL deionized H_2O was diluted with 0.1 M PBS (pH = 7.4) to a total volume of 1 mL. This results in 0.1 mg **Fe-L**, **Ni-L**, **Fe-CP** or **Ni-CP** in 1 mL 0.1 M PBS in the cell. This dispersion of the ligands and CPs was used for zeta potential measurements.

Calculation formula of electrical conductivity. Electrical conductivity (σ) measures a material's ability to conduct electrical current. Measuring σ typically requires incorporating the material of interest into an electronic device, typically a resistor, and measuring the electrical conductance (G), length (L), and cross-sectional area (A) of the conduction channel, and the calculation formula is as following:[8]

$$\sigma = G\frac{L}{A} \qquad (1)$$

Calculation formula of the limit of detection (LOD). According to the definition of the International Union of Pure and Applied Chemistry (IUPAC), the limit of detection (LOD) can be estimated according to the equation:[9]

$$LOD = K \times \frac{S_b}{m} \qquad (2)$$

Where S_b is the standard deviation of the responses to blank solutions (without analytes); m is the slope of the calibration plot in the linear analyte detection range; and K is a numerical factor chosen according to the desired confidence level (K=3).

CV measurements of the ligands and CPs modified electrodes in acetonitrile. The electrolyte was an acetonitrile solution of 0.1 M *n*-tetrabutylammonium hexafluorophosphate (*n*-Bu_4NPF_6), and the CV measurements of the ligands and CPs modified GCE in acetonitrile

were carried out in a three-electrode system with Pt wire as counter electrode and an Ag/Ag^+ electrode (0.01 M $AgNO_3$ and 0.1 M *n*-Bu_4NPF_6 in acetonitrile) as the reference electrode. Before the CV measurements, the electrolyte solution was deoxygenated with N_2 for 30 min, and ferrocene (Fc) was used as the internal potential standard.

Interference test: The concentrations of the interferents are as follows, 10 μM DA, 20 μM UA, 20 μM AA, 20 μM Glu, 20 μM Cys, 20 μM GSH, 20 μM H_2O_2 and 20 μM $NaNO_2$.

Preparation of the artificial urine. The artificial urine solution contained 1.1 mM lactic acid, 2.0 mM citric acid, 25 mM sodium bicarbonate, 170 mM urea, 2.5 mM calcium chloride, 90 mM sodium chloride, 2.0 mM magnesium sulfate, 10 mM sodium sulfate, 7.0 mM potassium dihydrogen phosphate, 7.0 mM dipotassium hydrogen phosphate, and 25 mM ammonium chloride all mixed in Millipore-purified water. The pH of the solution was adjusted to 6.0 by addition of 1.0 M hydrochloric acid.[10]

Calculation of diffusion coefficient and heterogenous electron transfer rate. The peak current, i_p, is directly proportional to the analyte concentration, C, as described by the simplified Randles-Sevcik equation at 25 ℃.[11]

$$i_p = k \times n^{3/2} \times A \times \sqrt{Dv} \times C \qquad (3)$$

In this equation, k is a constant of 2.69×10^5 (C mol^{-1} $V^{-½}$), n is the number of electrons transferred during the redox event, A is the area of electrode (cm^2), D is the diffusion coefficient of the analyte (cm^2 s^{-1}) and ν is the scan rate at which the potential is swept (V s^{-1}). ν was measured over a range of scan rates from 10 to 1000 mV s^{-1}. From the slope of the plots of current (i_p) versus the square-root of the scan rate, the diffusion coefficient of ligands and CPs can be obtained according to the following equation:

$$D = \frac{(\frac{i_p}{\sqrt{v}})^2}{k^2 \times n^3 \times A^2 \times C^2} = \frac{Slope^2}{k^2 \times n^3 \times A^2 \times C^2} \qquad (4)$$

where A is equal to 0.07 cm^2 (area of a 3 mm glassy carbon electrode), n is 2 for DA.

$$logk_0 = -0.48\alpha + 0.52 + \log[nF\alpha VcD/2.303RT]^{1/2} \quad (5)$$

For DA, the Gileadi method (equation 3) was used to calculate the heterogenous electron transfer rate k_0 (cm s^{-1});[8] α is 0.5, n is 2, F is the Faraday constant (C mol^{-1}), V_c is the critical scan rate (V s^{-1}) (see Fig. S16), D is the diffusion coefficient (cm^2 s^{-1}), R is the gas constant of 8.314 (J K^{-1} mol^{-1}), T is the room temperature 298 K.[12]

Determination of surface concentration of electroactive metal sites in CPs or ligands on electrodes. To estimate the surface concentration of electroactive Fe or Ni in the CPs or the ligands, CV tests of the CPs or ligands modified electrodes in N_2 saturated 0.1 M pH 7.4 PBS with scan rate between 20 to 120 mV s^{-1} were conducted. The peak current shows a linear dependence on the scan rate. Calculation of surface concentration (τ) of the electroactive metal in CPs or ligands was performed by the following equation:

$$slope = \frac{n^2F^2A\tau}{4RT}$$

where n is the number of electrons involved (n = 1), F is the Faraday constant, A is geometrical surface area of the electrode (0.07 cm^2), τ is the surface concentration, R is the gas constant, T is test temperature (298 K).[13]

Redox process of DA. The electrochemical redox reaction of DA to dopamine quinone (DAQ) involved in two electron and two protons process is as follows:[14]

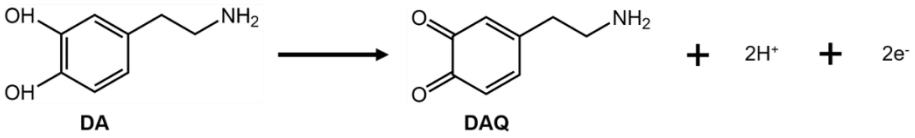

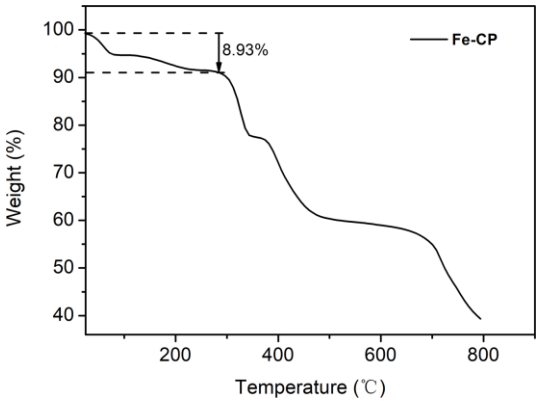

Fig. S1 TGA curve of **Fe-CP**.

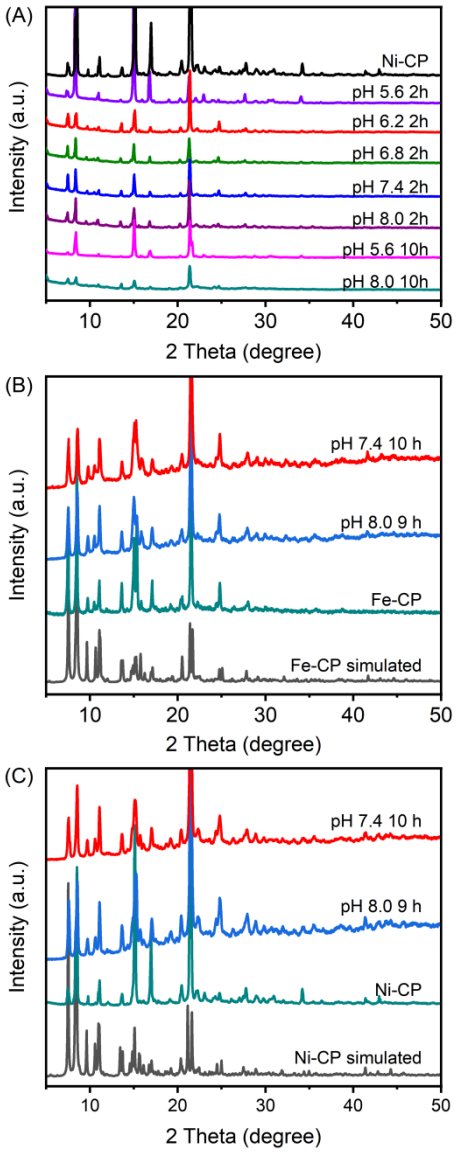

Fig. S2 PXRD patterns of (A, C) **Ni-CP** and (B) **Fe-CP** after being soaked in 0.1 M PBS solution at varied pH for determined time.

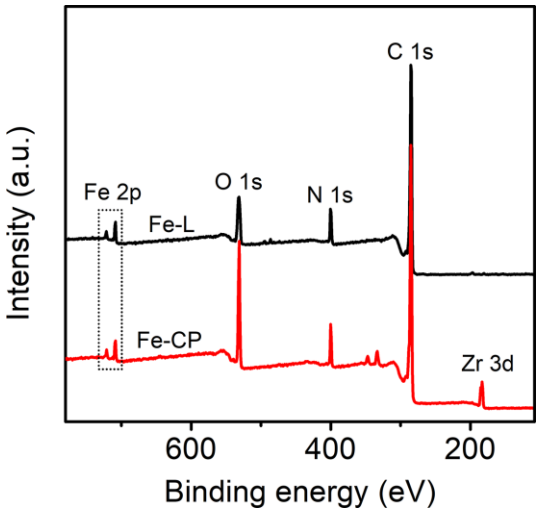

Fig. S3 XPS survey scan of **Fe-L** and **Fe-CP**.

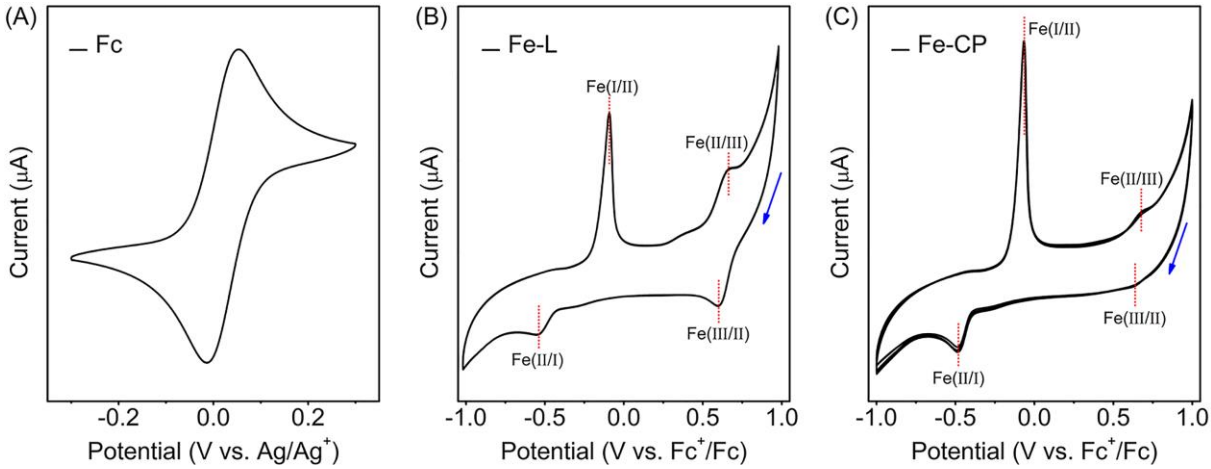

Fig. S4 CV curves of (A) GCE in 0.1 M *n*-Bu_4NPF_6 acetonitrile solution containing 1 mM ferrocene (Fc), (B) **Fe-L**, (C) **Fe-CP** modified electrodes in 0.1 M *n*-Bu_4NPF_6 acetonitrile saturated with N_2 at scan rate of 0.1 V s^{-1} (blue arrow indicates the scan direction).

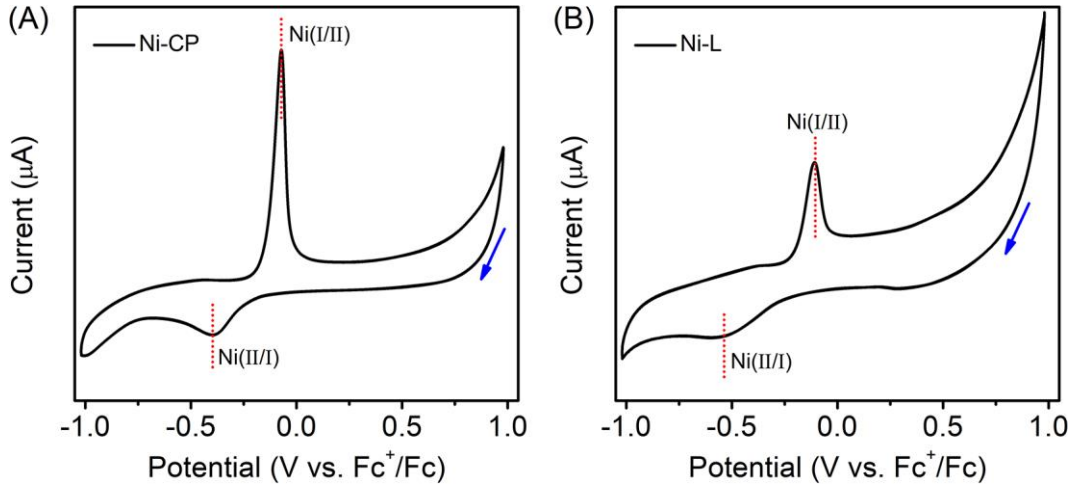

Fig. S5 CV curves of (A) **Ni-CP** and (B) **Ni-L** modified electrodes in 0.1 M *n*-Bu_4NPF_6 acetonitrile saturated with N_2 at scan rate of 0.1 V s^{-1} (blue arrow indicates the scan direction).

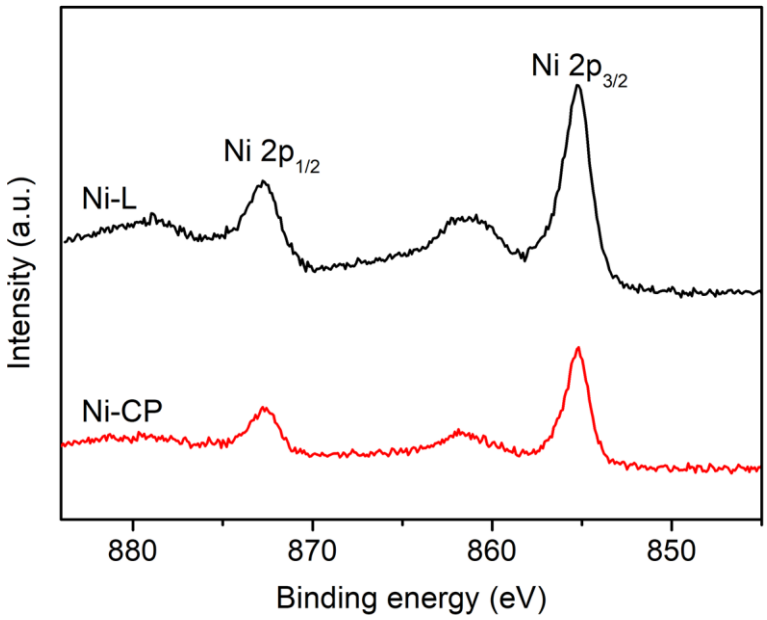

Fig. S6 XPS spectra of Ni 2p of **Ni-L** and **Ni-CP**.

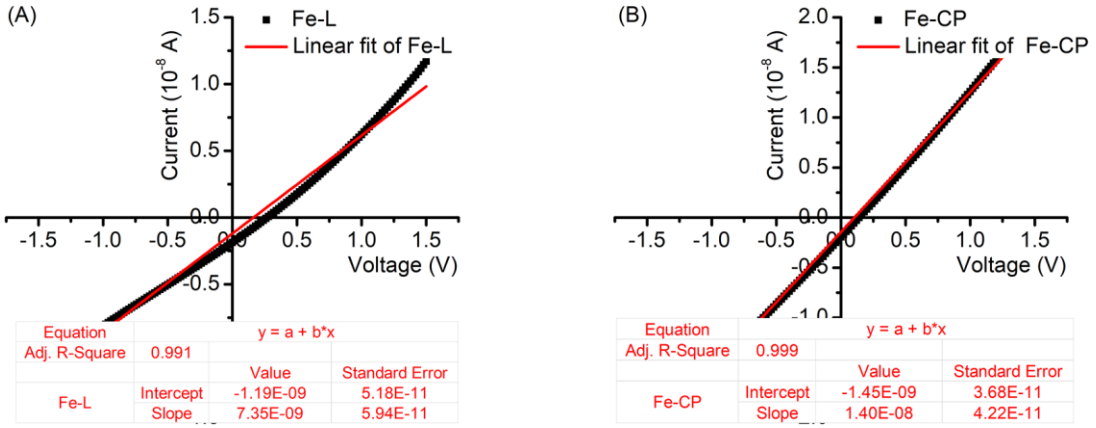

Equation	y = a + b*x		
Adj. R-Square	0.991		
		Value	Standard Error
Fe-L	Intercept	-1.19E-09	5.18E-11
	Slope	7.35E-09	5.94E-11

Equation	y = a + b*x		
Adj. R-Square	0.999		
		Value	Standard Error
Fe-CP	Intercept	-1.45E-09	3.68E-11
	Slope	1.40E-08	4.22E-11

Fig. S7 Current versus voltage plot for pressed pellets of (A) **Fe-L** and (B) **Fe-CP**. The scan was performed from -1.5 V to 1.5 V at room temperature with a scan rate of 50 mV s^{-1}.

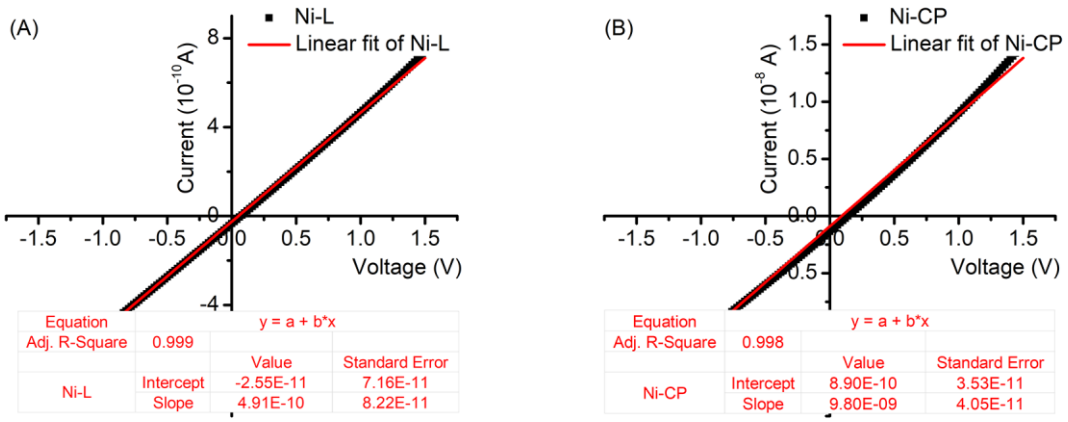

Equation	y = a + b*x		
Adj. R-Square	0.999		
		Value	Standard Error
Ni-L	Intercept	-2.55E-11	7.16E-11
	Slope	4.91E-10	8.22E-11

Equation	y = a + b*x		
Adj. R-Square	0.998		
		Value	Standard Error
Ni-CP	Intercept	8.90E-10	3.53E-11
	Slope	9.80E-09	4.05E-11

Fig. S8 Current versus voltage plot for pressed pellets of (A) **Ni-L** and (B) **Ni-CP**. The scan was performed from -1.5 V to 1.5 V at room temperature with a scan rate of 50 mV s^{-1}.

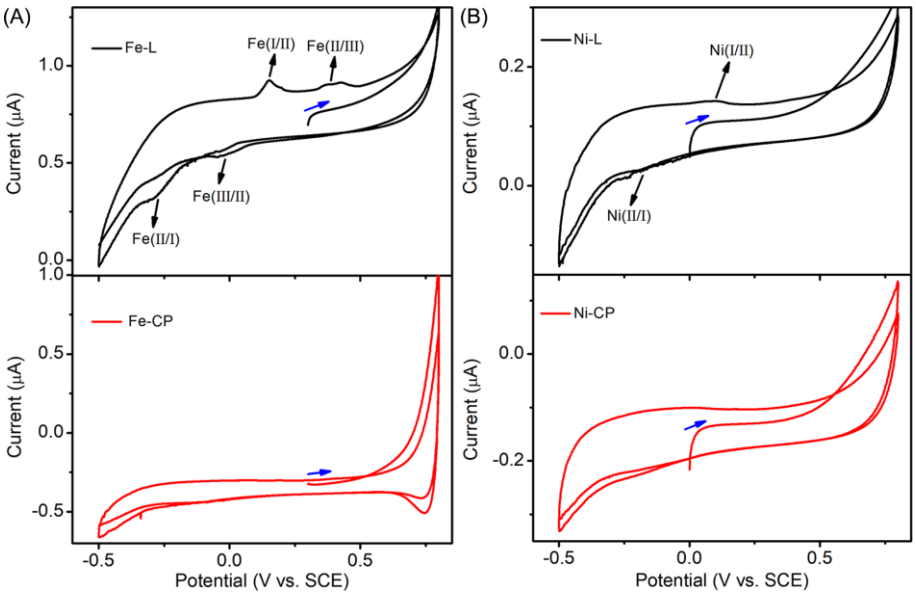

Fig. S9 CV curves recorded on the (A) **Fe-L** and **Fe-CP** modified electrodes, and (B) **Ni-L** and **Ni-CP** modified electrodes in 0.1 M pH 7.4 PBS saturated with N_2 at a scan rate of 5 mV s^{-1} (blue arrow indicates the scan direction).

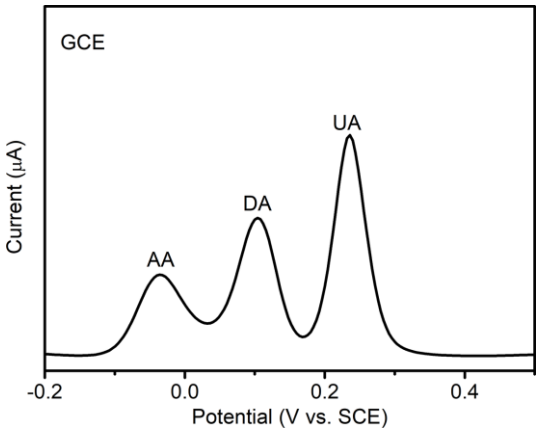

Fig. S10 DPV responses of GCE in the presence of 100 μM DA, 100 μM AA and 100 μM UA in 0.1 M PBS at pH 7.4.

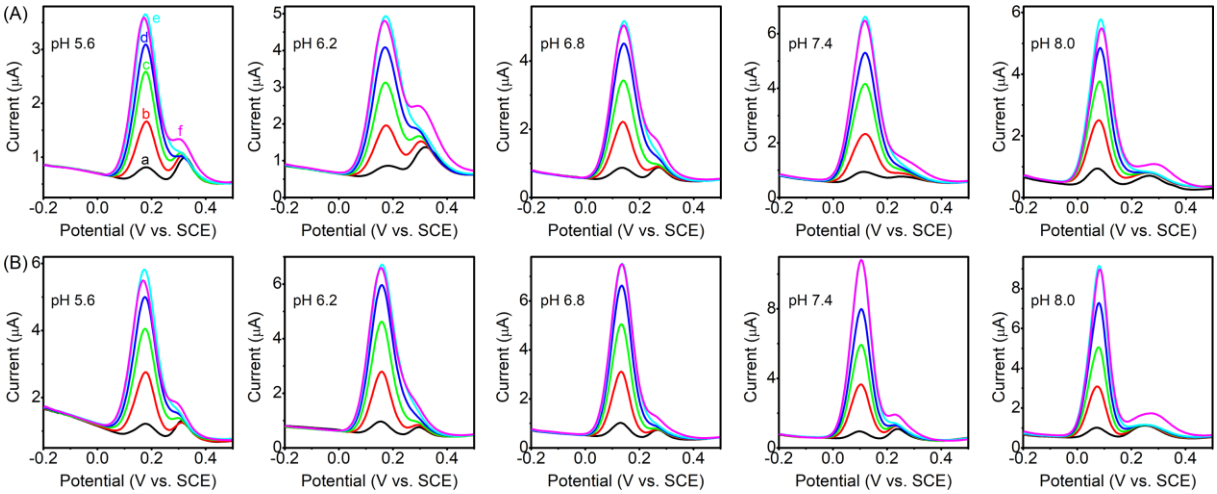

Fig. S11 DPV responses of (A) **Ni-L** and (B) **Ni-CP** modified electrodes in different pH 0.1 M PBS in the presence of (a) 10 μM DA + 100 μM AA + 100 μM UA, (b) 50 μM DA + 100 μM AA + 100 μM UA, (c) 100 μM DA + 100 μM AA + 100 μM UA, (d) 150 μM DA + 100 μM AA + 100 μM UA, (e) 200 μM DA + 100 μM AA + 100 μM UA, (f) 200 μM DA + 100 μM AA + 200 μM UA.

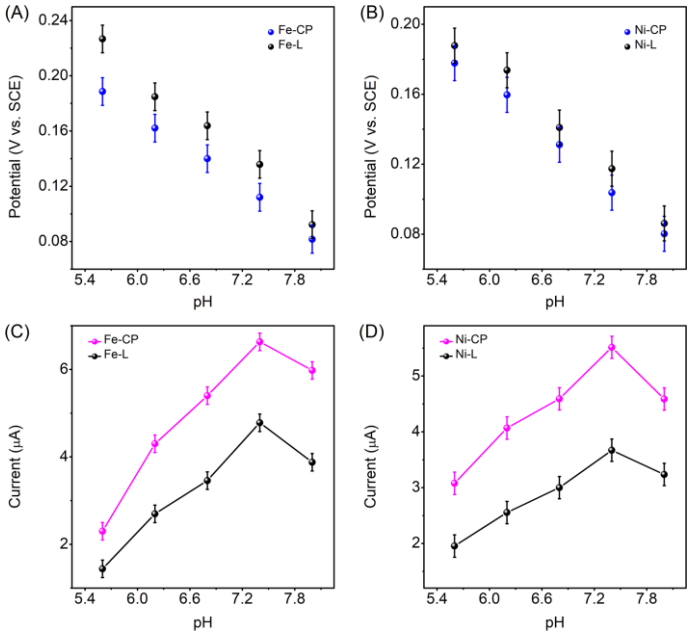

Fig. S12 Plots of the oxidation peak potential versus pH for (A) **Fe-L** and **Fe-CP** modified electrodes and (B) **Ni-L** and **Ni-CP** modified electrodes in 0.1 M PBS at pH 7.4 containing 100 μM DA. Plots of the oxidation peak current versus pH for (C) **Fe-L** and **Fe-CP** modified electrodes and (D) **Ni-L** and **Ni-CP** modified electrodes in 0.1 M PBS at pH 7.4 containing 100 μM DA.

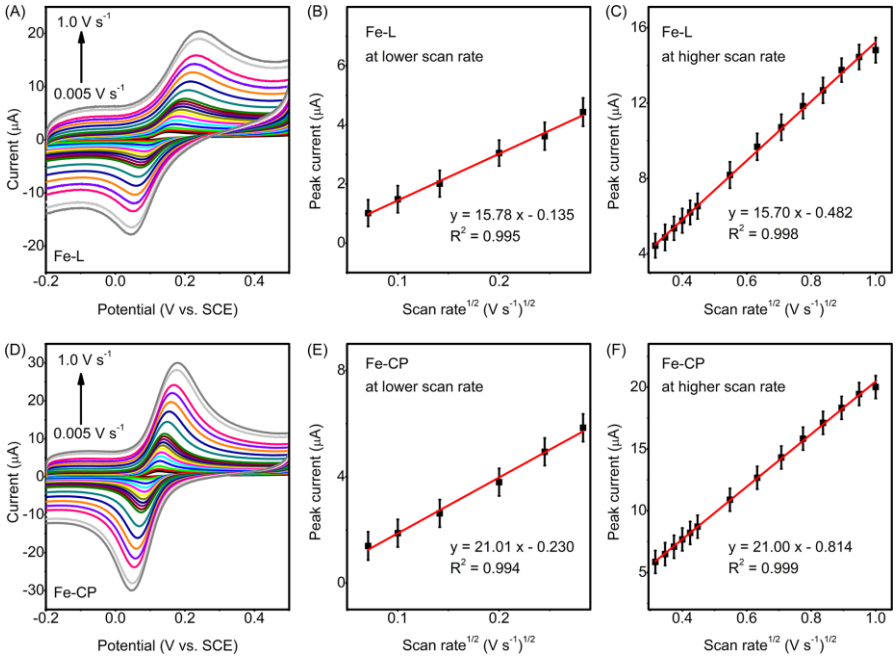

Fig. S13 CV curves of (A) **Fe-L** and (D) **Fe-CP** modified electrodes in 0.1 M pH 7.4 PBS containing 100 μM DA at different scan rates ranging from 0.005 V s^{-1} to 1.0 V s^{-1}, and (B, C, E, F) their corresponding Randles-Sevcik plot of the current versus the scan $rate^{1/2}$.

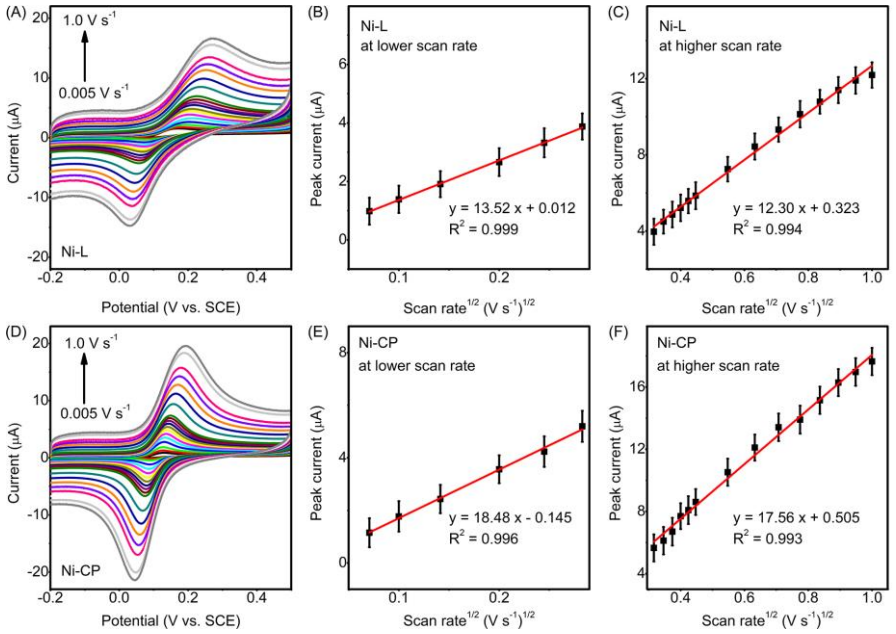

Fig. S14 CV curves of (A) **Ni-L** and (D) **Ni-CP** modified electrodes in 0.1 M pH 7.4 PBS containing 100 μM DA at different scan rates ranging from 0.005 V s^{-1} to 1.0 V s^{-1}, and (B, C, E, F) their corresponding Randles-Sevcik plot of the current versus the scan $rate^{1/2}$.

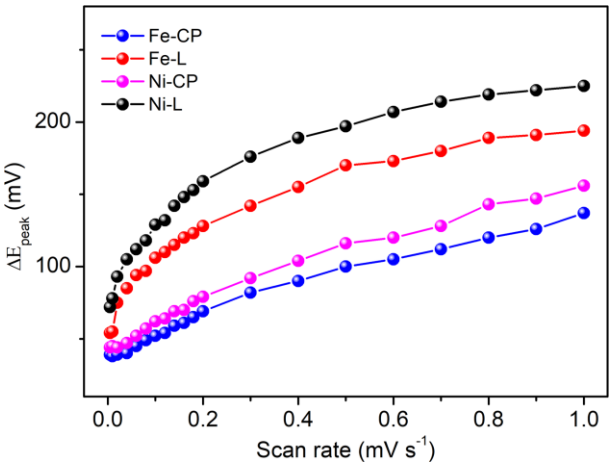

Fig. S15 Peak-to-peak potential separation recorded for the ligands and CPs modified electrodes at different scan rate in 0.1 M pH 7.4 PBS containing 100 μM DA (based on Figs. S13 and S14).

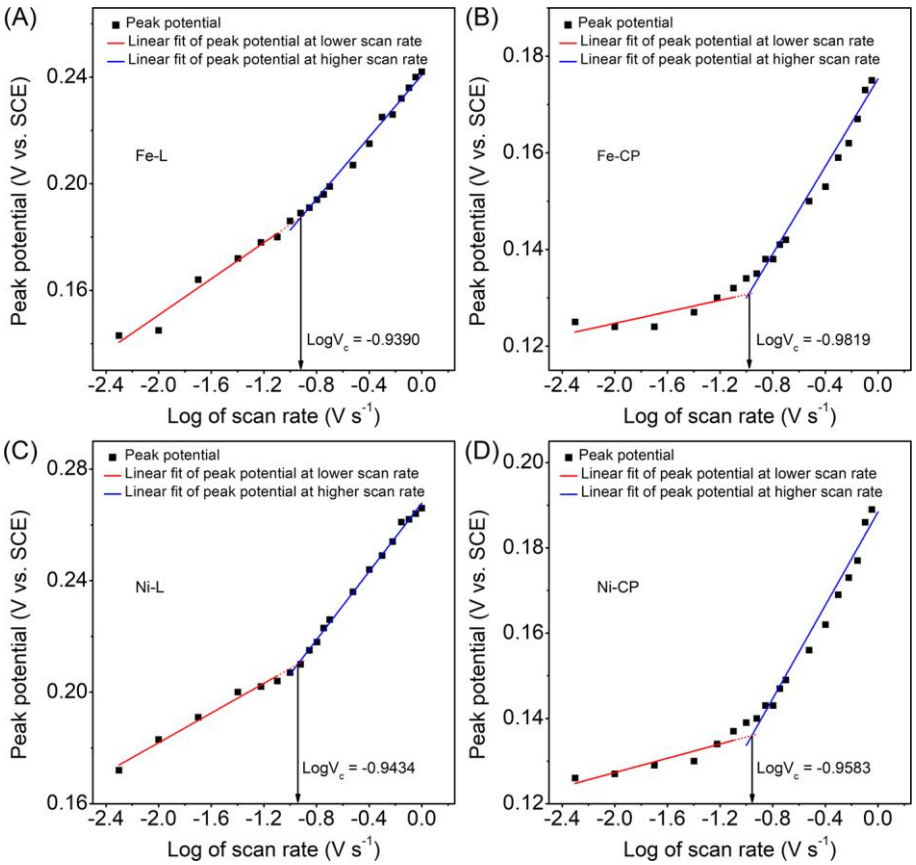

Fig. S16 Plots between log of peak potential versus log of scan for critical scan rate (V_c) based on the Gileadi method[8] (based on Figs. S13 and S14).

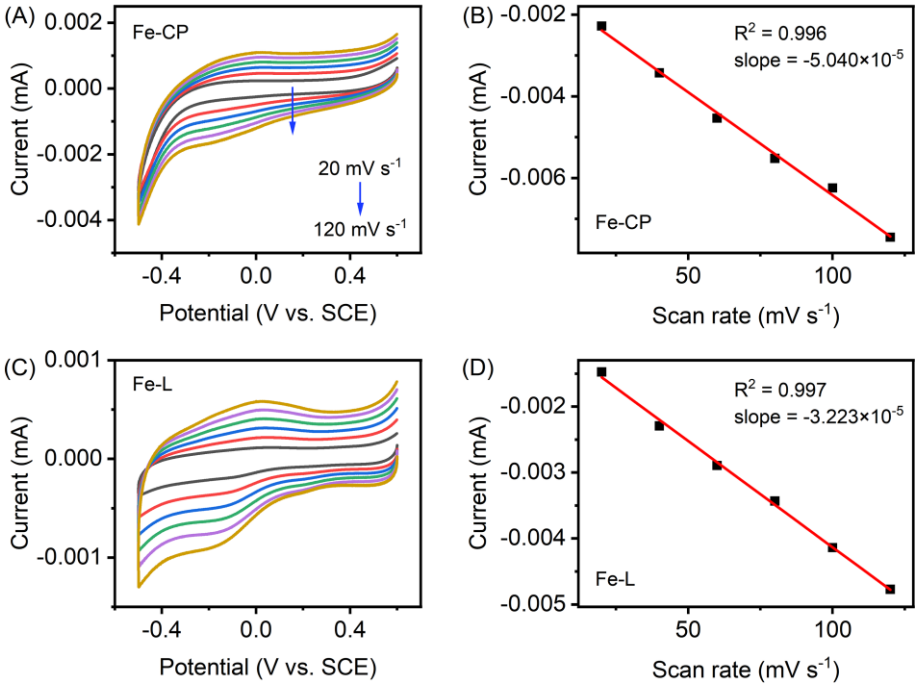

Fig. S17 Scan rate dependence of CV response of (A) **Fe-CP** and (C) **Fe-L**. (b) Peak current of the CV of (B) **Fe-CP** and (D) **Fe-L** as a function of scan rate.

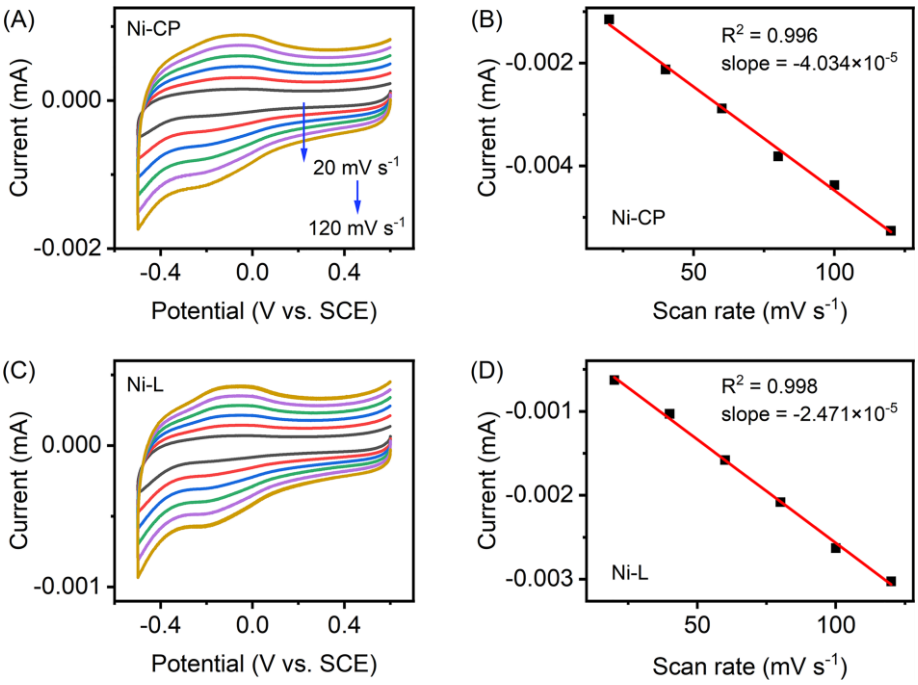

Fig. S18 Scan rate dependence of CV response of (A) **Ni-CP** and (C) **Ni-L**. (b) Peak current of the CV of (B) **Ni-CP** and (D) **Ni-L** as a function of scan rate.

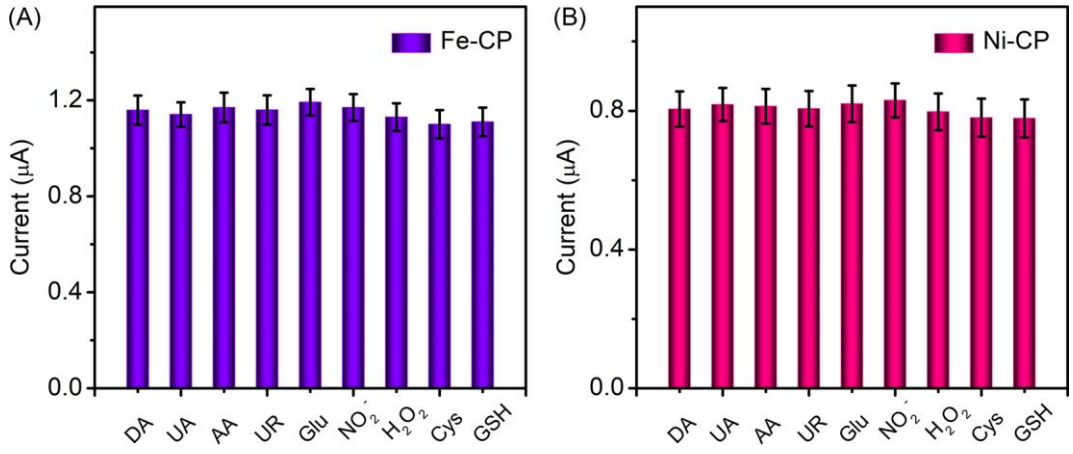

Fig. S19 DPV response of interference test of the (A) **Fe-CP** and (B) **Ni-CP** modified electrodes towards 10 μM DA in the presence of different interferents in 0.1 M pH 7.4 PBS.

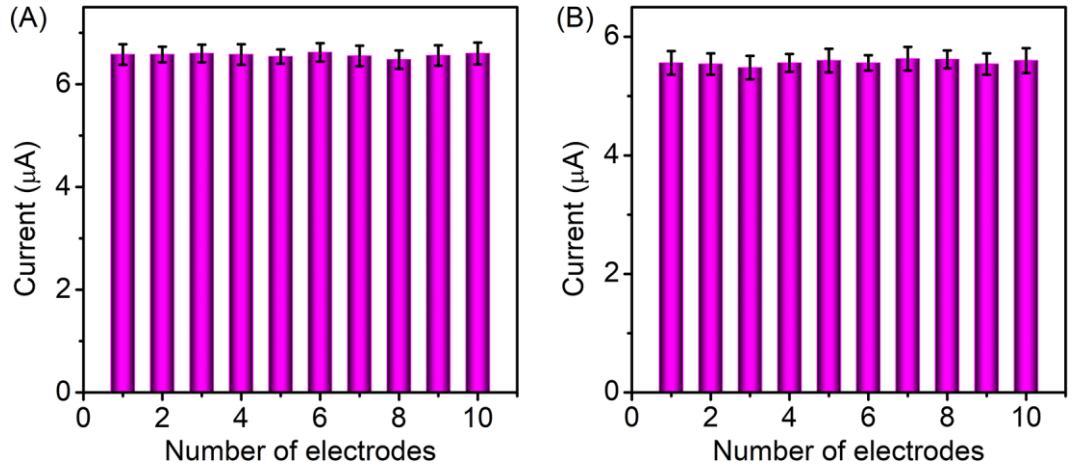

Fig. S20 Variation in the oxidation peak currents of 10 individual (A) **Fe-CP** and (B) **Ni-CP** modified electrodes towards 100 μM DA in 0.1 M pH 7.4 PBS.

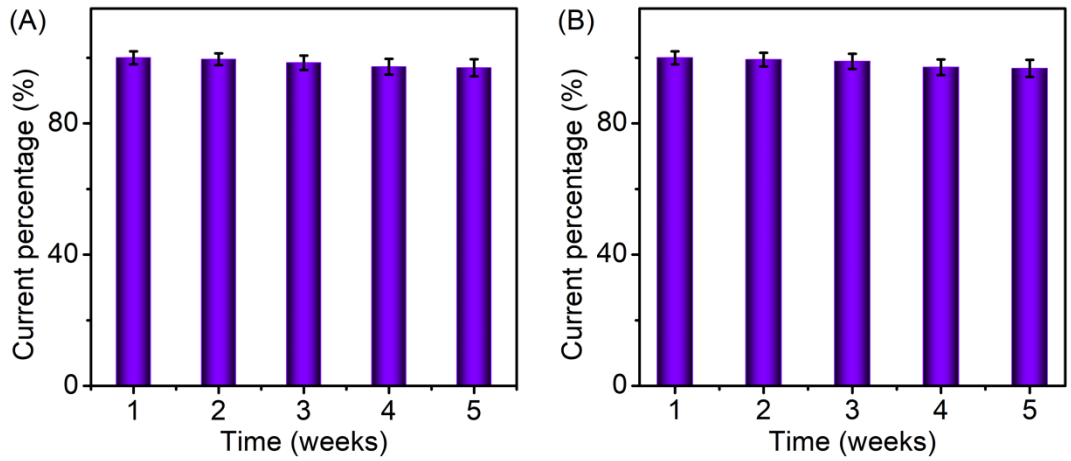

Fig. S21 Stability results of (A) **Fe-CP** and (B) **Ni-CP** modified electrodes to 100 μM DA tested every 7 days by DPV in one month.

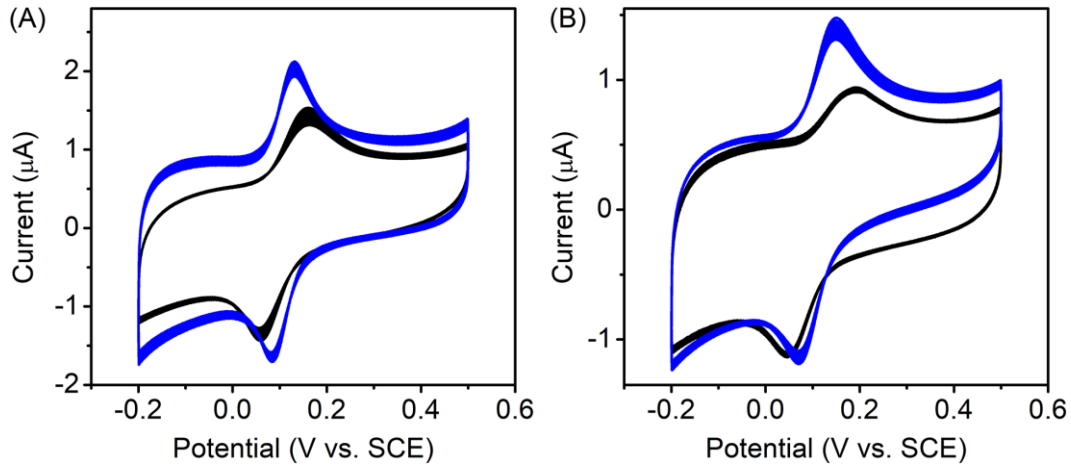

Fig. S22 CV curves recorded after 90 cycles of (A) **Fe-L** (black) and **Fe-CP** (blue), and (B) **Ni-L** (black) and **Ni-CP** (blue) modified electrodes in 0.1 M pH 7.4 PBS containing 10 μM DA.

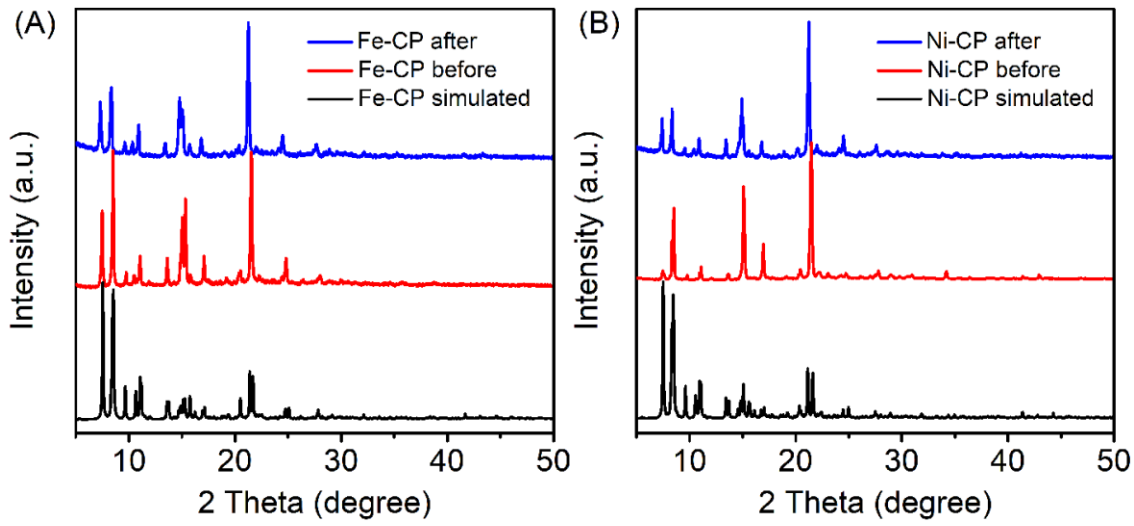

Fig. S23 PXRD patterns of (A) **Fe-CP** and (B) **Ni-CP** after electrochemical DA detection in 0.1 M pH 7.4 PBS.

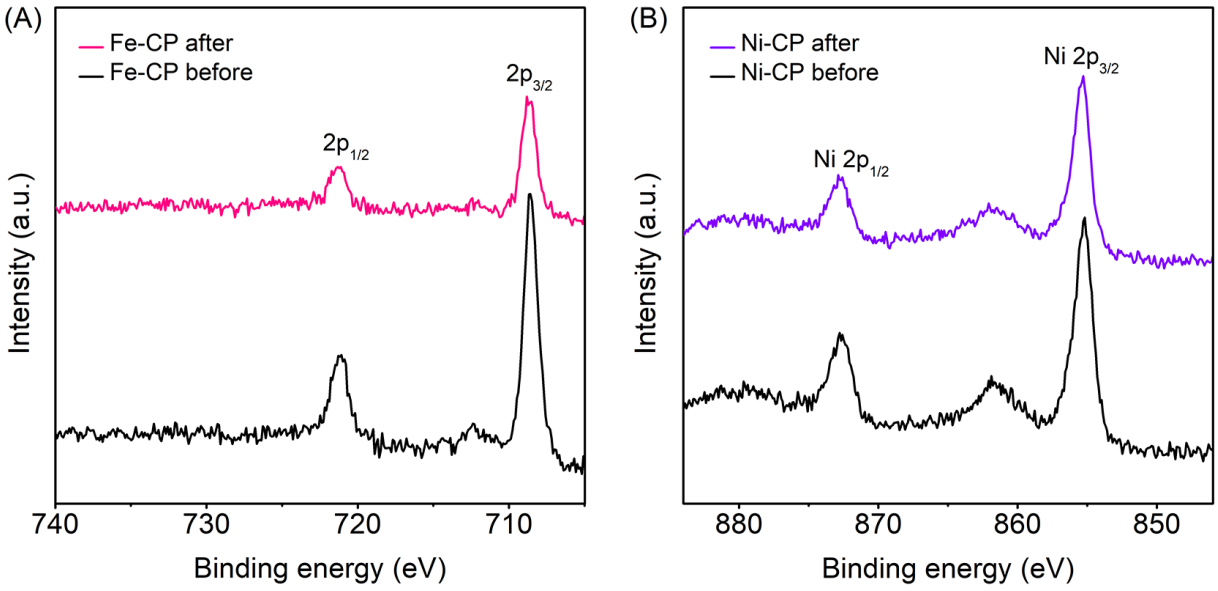

Fig. S24 XPS spectra of (A) Fe 2p of **Fe-CP** and (B) Ni 2p of **Ni-CP** after electrochemical DA detection in 0.1 M pH 7.4 PBS.

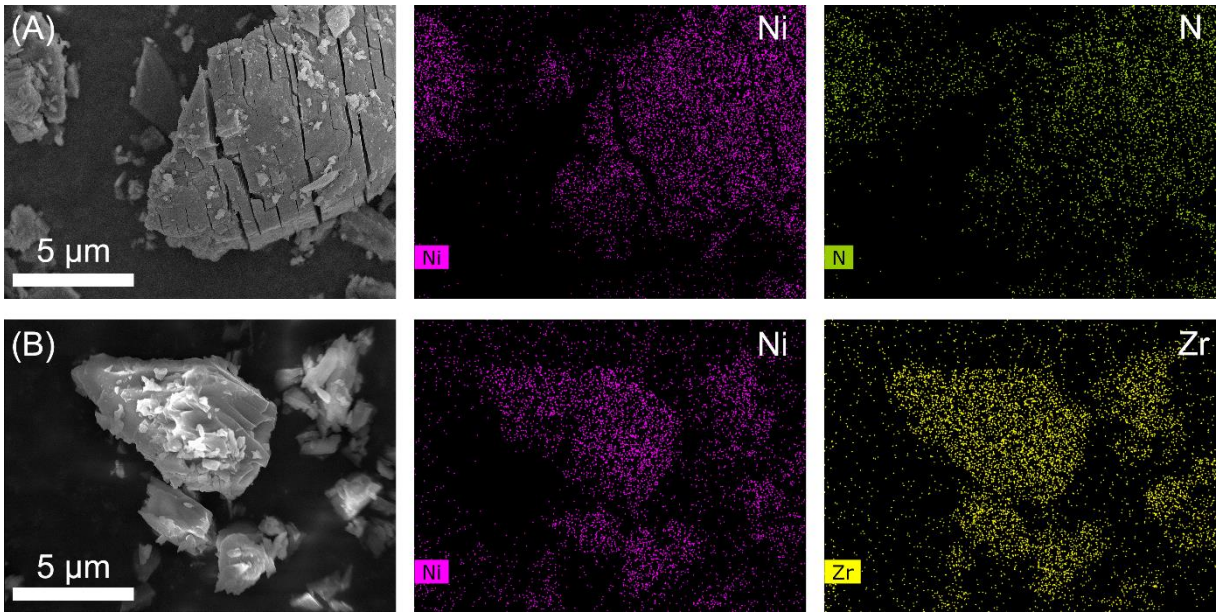

Fig. S25 SEM and corresponding elemental mapping images of (A) **Ni-L** and (B) **Ni-CP** after the electrochemical detection of DA.

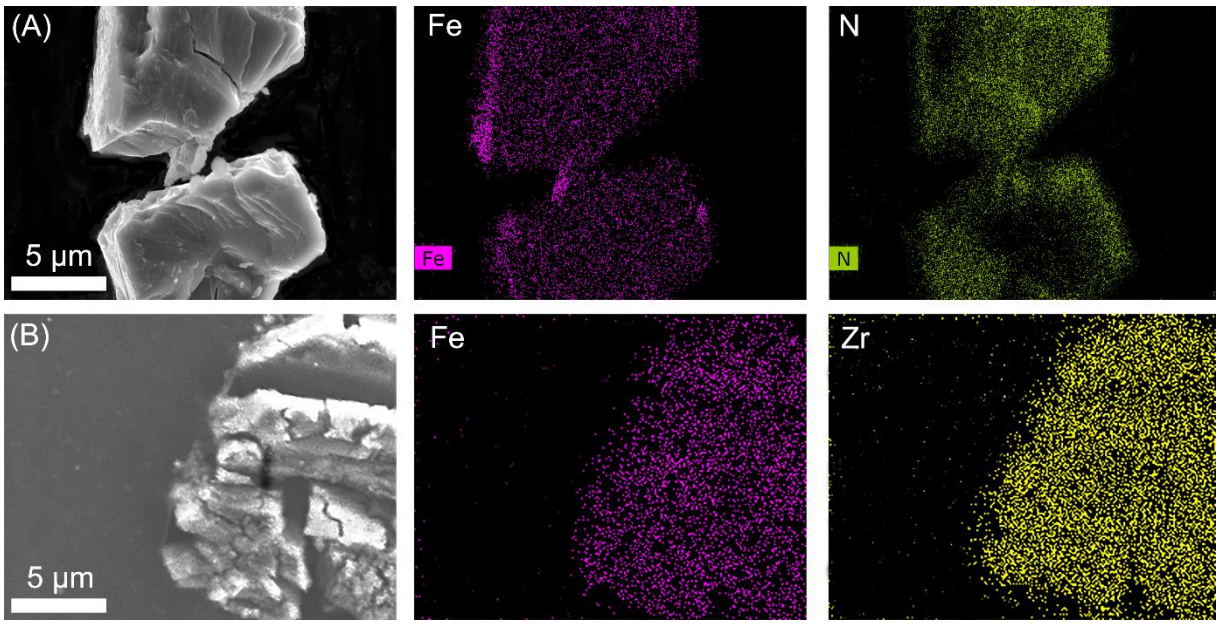

Fig. S26 SEM and corresponding elemental mapping images of (A) **Fe-L** and (B) **Fe-CP** after the electrochemical detection of DA.

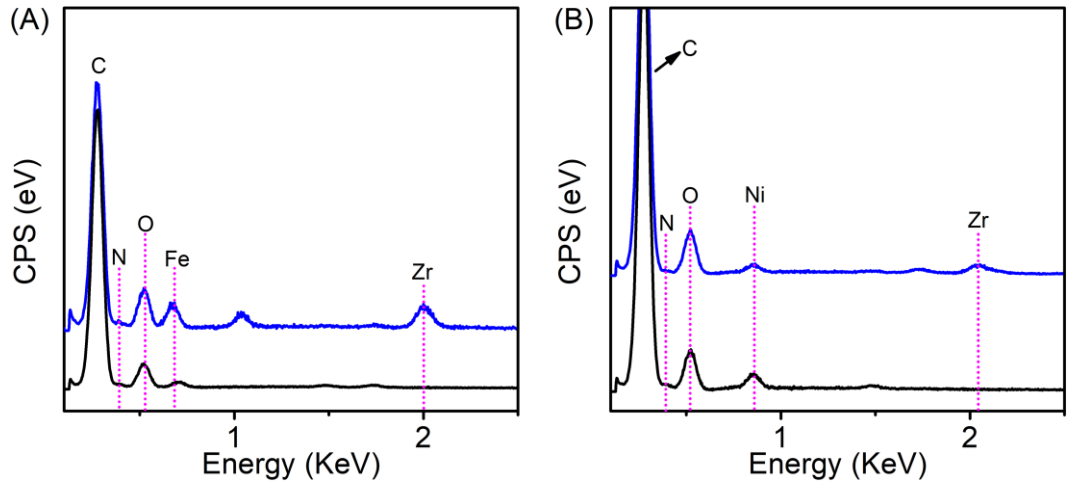

Fig. S27 EDS spectra of (A) **Fe-L** (black) and **Fe-CP** (blue), and (B) **Ni-L** (black) and **Ni-CP** (blue) after the electrochemical detection of DA.

Table S1 Crystal data and structure refinements for **Fe-CP**.

Compound	**Fe-CP**
Formula	$C_{48}H_{32}FeN_6O_{12}Zr$
Formula weight	1031.86
Crystal system	Triclinic
Space group	*P*-1
a (Å)	23.216(3)
b (Å)	23.535(3)
c (Å)	26.103(3)
α (°)	95.628(6)
β (°)	90.075(6)
γ (°)	90.757(7)
V ($Å^3$)	14192(3)
Z	12
D_c (g cm^{-3})	1.449
μ (mm^{-1})	3.286
F (000)	6288
Data collected	126750
Unique reflections	48419
Goodness-of-fit	1.079
R_1[a] [$I > 2\sigma(I)$]	0.1310
wR_2[b] [$I > 2\sigma(I)$]	0.2844

[a] $R_1 = \Sigma||F_o| - |F_c||/\Sigma|F_o|$.

[b] $wR_2 = |\Sigma w\,(|F_o|^2 - |F_c|^2)\,|/\Sigma|w(F_o)^2|^{1/2}$, where $w = 1/[\sigma^2(F_o^2) + (aP)^2 + bP]$. $P = (F_o^2 + 2F_c^2)/3$

Table S2 Zeta potential analysis of the ligands and CPs dispersion in 0.1 M PBS with different pH.

	Observed zeta potential (mV)			
	Fe-L	**Fe-CP**	**Ni-L**	**Ni-CP**
pH 5.6	-8.9	-12.5	-8.6	-9.7
pH 6.2	-10.1	-11.0	-8.2	-10.1
pH 6.8	-10.4	-11.3	-8.7	-9.6
pH 7.4	-10.3	-11.6	-8.9	-9.4
pH 8.0	-10.5	-11.2	-10.6	-9.9

Table S3 The shape parameters of the ligands and CPs and their electrical conductivity.

	Fe-L	**Fe-CP**	**Ni-L**	**Ni-CP**
Length (mm)	3.95	3.93	3.73	3.88
Width (mm)	0.71	1.08	1.00	1.37
Thickness (mm)	0.370	0.492	0.241	0.376
Cross-sectional area (mm^2)	0.263	0.531	0.241	0.515
Electrical conductance (S)	7.35×10^{-9}	1.40×10^{-8}	4.91×10^{-10}	9.80×10^{-9}
Electrical conductivity (S cm^{-1})	1.10×10^{-6}	1.04×10^{-6}	7.60×10^{-7}	7.38×10^{-7}

Table S4 The concentration of the surface electrochemical active sites of the CPs or ligands modified electrode (5 uL 1 mg mL^{-1} of CP or ligand suspension was dropped on the GCE).

	Calculated Fe sites (mmol cm^{-2})	**Loaded Fe sites (by ICP)** (mmol cm^{-2})	**Fe sites found by CV** (mmol cm^{-2})	**Fe sites by CV / Loaded Fe sites** (%)
Fe-CP	6.922×10^{-5}	5.180×10^{-5}	7.660×10^{-7}	1.48
Fe-L	9.390×10^{-5}	7.060×10^{-5}	4.901×10^{-7}	0.69
	Calculated Ni sites (mmol cm^{-2})	**Loaded Ni sites (by ICP)** (mmol cm^{-2})	**Ni sites found by CV** (mmol cm^{-2})	**Ni sites by CV / Loaded Ni sites** (%)
Ni-CP	6.230×10^{-5}	4.515×10^{-5}	6.128×10^{-7}	1.36
Ni-L	8.369×10^{-5}	6.218×10^{-5}	3.757×10^{-7}	0.60

Table S5 The electroanalytical DA performances of CPs modified on GCE.

	Method	Sensitivity ($\mu A\ \mu M^{-1}cm^{-2}$)	Linear range (μM)	LOD (μM)	Ref.
Ni_3HITP_2	DPV	N/A	0.04-200	0.424	15
Ni_3HHTP_2	DPV	N/A	0.06-200	0.061	15
Cu_3HITP_2	DPV	N/A	2-200	2.3	15
Cu_3HITP_2	DPV	N/A	0.14-200	0.194	15
IL-RGO/ZIF-8	DPV	0.81	0.1-100	0.035	16
Fe_2Ni MIL-88B	i-t	124.7	1.2-1800	0.40	17
Ni-MOF	DPV	3	0.2-100	0.06	18
Pxa/Au/Cu-TCPP	DPV	0.3	5-125	1.0	19
Sulfo-MIL-101-GPE	CV	2.55	0.07-100	0.043	20
HKUST-1	DPV	0.84	12.5-175	0.11	21
Fe-CP	DPV	1.12	0.05-250	0.040	This work
Ni-CP	DPV	0.86	0.1-300	0.062	This work

N/A: not available

References

1 E. C. Constable, E. L. Dunphy, C. E. Housecroft, M. Neuburger, S. Schaffner, F. Schaper and S. R. Batten, *Dalton trans.*, 2007, **38**, 4323-4332.

2 X. Y. Zhang, C. F. Xie, S. Q. Wang, X. M. Cheng, Y. Zhang, Y. Zhao, Y. Lu and W. Y. Sun, *Inorg. Chem.*, 2022, **61**, 1590-1596.

3 Y. N. Wang, T. Liu, L. X. Chen and D. B. Chao, *Inorg. Chem.*, 2021, **60**, 5590-5597.

4 SAINT. *Program for Data Extraction and Reduction*. Bruker AXS, Inc.,Madison, WI 2001.

5 G. M. Sheldrick and SADABS, *Program for Empirical Adsorption Correction of Area Detector Data*. University of Gottingen, Gottingen, Germany, 2003.

6 G. M. Sheldrick, *SHELXS-2018, Program for the Crystal Structure Solution*. University of Gottingen, Gottingen, Germany, 2018.

7 P. Van der Sluis and A. L. Spek, *Acta Cryst.*, 1990, **A46**, 194-201.

8 Y. Zhou, Q. Hu, F. Yu, G. Y. Ran, H. Y. Wang, N. D. Shepherd, D. M. D'Alessandro, M. Kurmoo and J. L. Zuo, *J. Am. Chem. Soc.*, 2020, **142**, 20313-20317.

9 G. L. Long and J. D. Winefordner, *Anal. Chem.*, 1983, **55**, 712A-724A.

10 A. K. Ellerbee, S. T. Phillips, A. C. Siegel, K. A. Mirica, A. W. Martinez, P. Striehl, N. Jain, M. Prentiss and G. M. Whitesides, *Anal. Chem.*, 2009, **81**, 8447-8452.

11 A. J. Bard and L. R. Faulkner, *Electrochemical Methods: Fundamentals and Applications*, Wiley, New York, 2001.

12 H. Muhammad, I. A. Tahiri, M. Muhammad, Z. Masood, M. A. Versiani, O. Khaliq, M. Latif and M. Hanif, *J. Electroanal. Chem.*, 2016, **775**, 157-162.

13 B. Han, Y. C. Jin, B. T. Chen, W. Zhou, B. Q. Yu, C. Y. Wei, H. L. Wang, K. Wang, Y. L. Chen, B. L. Chen, J. Z. Jiang, *Angew. Chem. Int. Ed.*, 2022, **61**, e202114244.

14 A. Ciszewski and G. Milczarek, *Anal. Chem.*, 1999, **71**, 1055-1061.

15 M. Ko, L. Mendecki, A. M. Eagleton, C. G. Durbin, R. M. Stolz, Z. Meng and K. A. Mirica, *J. Am. Chem. Soc.*, 2020, **142**, 11717-11733.

16 L. Cheng, Y. J. Fan, X. C. Shen and H. Liang, *J. Nanomater.*, 2019, **2019**, 8936095.

17 C. Q. Duan and J. B. Zheng, *J. Electrochem. Soc.*, 2019, **166**, B942-B947.

18 Z. X. Huang, L. J. Zhang, P. F. Cao, N. Wang and M. Lin, *Ionics*, 2021, **27**, 1339-1345.

19 Z. W. Qiu, T. Yang, R. Gao, G. F. Jie and W. G. Hou, *J. Electrochem. Soc.*, 2019, **835**, 123-129.

20 L. L. Gao, W. J. Sun, X. M. Yin, R. Bu and E. Q. Gao, *Microchim. Acta*, 2019, **186**, 762.

21 F. A. Sofi, M. A. Bhat and K. Majid, *New J. Chem.*, 2019, **43**, 3119-3127.